# Thermal attractor in chaotic convection with high-Prandtl-number fluids

Alain P. Vincent and David A. Yuen
*Minnesota Supercomputer Institute, Minneapolis, Minnesota 55415*
*and Department of Geology and Geophysics, University of Minnesota, Minneapolis, Minnesota 55455*
(Received 14 September 1987)

The onset of chaotic convection in large-Prandtl-number fluids has been found to occur in the form of elongated cells with aperiodic boundary-layer instabilities. The dynamics of this phenomenon has been monitored in the physical domain, and also in the spectral and phase spaces. In order to describe more precisely the underlying mechanisms of chaotic thermal convection, we find it useful to introduce the notion of "thermal attractor" in the physical domain and to conduct a systematic study of the evolution of the spectral energy surfaces. We propose here a relationship between this thermal attractor and the presence of a strange attractor in the phase space.

Much progress has been made in the elucidation of the onset of chaotic thermal convection.[1,3] The effects of a large-aspect-ratio configuration on the transition process have been demonstrated for low-Prandtl-number fluids.[4,5] A truncated modal model[6] has been used to study the transition to time-dependent, large-scale flows for low Prandtl numbers.

Large-Prandtl-number convection has been a topic of intense study among geophysicists because of its application to mantle convection. The appearance of chaotic convection as a large-aspect-ratio, single-cell phenomenon, punctuated with recurring boundary-layer instabilities has been found in numerical solutions of large-Prandtl-number convection.[7] It has been determined in these convection flows that the transition to chaos occurs via oscillatory convection with two frequencies and involves a small number of relevant degrees of freedom.[8] Spatial patterns in temporal chaotic Rayleigh-Bénard convection are also of interest to physicists and remain an open problem of great current interest.[9]

Convection with infinite-Prandtl-number fluids is interesting in its own right because it contains only one nonlinear term, that due to thermal advection, in the Boussinesq regime. This facet permits one to focus on the only source of producing time-dependent transitions, leading to the chaotic stage. In this work we intend to focus on the energy partitioning among the different modes and to propose a mechanism responsible for producing thermal chaos in high-Prandtl-number convection, in which inertial effects can be neglected in the momentum equations.

The dimensionless equations representing infinite-Prandtl-number, Boussinesq thermal convection are given by

$$\nabla\cdot\mathbf{v}=0\ , \tag{1}$$

$$-\nabla p+\nabla^2\mathbf{v}+R\,\theta\hat{\mathbf{z}}=0\ , \tag{2}$$

$$\frac{\partial\theta}{\partial t}+(\mathbf{v}\cdot\nabla)\theta=\mathbf{v}\cdot\hat{\mathbf{z}}+\nabla^2\theta\ , \tag{3}$$

where $t$ is the time, $\mathbf{v}$ is the velocity, $\theta$ is the thermal deviation from the conductive profile, $p$ is the dynamical pressure, and $\hat{\mathbf{z}}$ is the unit vector aligned with gravity. In nondimensionalizing the equations we have used the layer depth $d$ for the length, the thermal diffusion time across $d$ for the time, and the temperature drop across the layer for temperature perturbations. The only parameter which determines the convection flow is the Rayleigh number $R$, the ratio between the buoyant energy liberated to the viscous dissipation. We will solve Eqs. (1)–(3) with stress-free boundaries for the top and bottom and periodic boundary conditions along the horizontal.

We employ a spectral code in the numerical computations. The unknowns are expanded in a Fourier-Chebyshev basis with the Fourier functions satisfying the periodic boundary conditions. The tau method[10] is used for enforcing the vertical boundary conditions of the temperature and momentum equations. We use the spectral-transform method for calculating explicitly in time the nonlinear thermal-advection term. Time stepping is done by a second-order, Adams-Bashforth, Cranck-Nicholson scheme. The principal reason for using the spectral method is to study in greater detail energy partitioning among the active modes in order to gain a better understanding of the nonlinear aspects of chaotic convection.

We have focused on one particular example in this paper. It is for an aspect-ratio-6 box with $R=3\times10^5$, which is about several hundred times supercritical. The initial condition chosen is a single-cell pattern obtained for a slightly supercritical Rayleigh number. We have used 187 complex Fourier functions and 46 Chebyshev polynomials. Increasing these to 335 Fourier and 82 Chebyshev functions does not cause any noticeable changes in the solution. Kinetic energy is computed as the average of the Euclidian norm of the velocity over the Chebyshev spectral space.

In Fig. 1 we show the evolution of the stream function $\psi$ and temperature fields in the physical domain between $t=0.2256$ and 0.2328. The stream function $\psi$ for incompressible flows is defined with $u=-\partial\psi/\partial z$ and $w=\partial\psi/\partial x$, where $x$ and $z$ are, respectively, the horizontal and vertical coordinates. Long-wavelength cells, punctuated by traveling boundary-layer instabilities, are clearly illustrated. This event can occur sometimes after

 

one or two overturn times (Fig. 2) at $t=0.204$. However, this phase lasts only briefly and the elongated cell returns at $t=0.2016$.

The presence of two cells in the physical domain comes from the nature of the periodic horizontal boundary conditions. We find that with the onset of chaotic convection horizontal symmetry is broken and each cell assumes a different configuration. Symmetry is also broken vertically but is not discernible in the physical domain because the frequencies involved are too high.

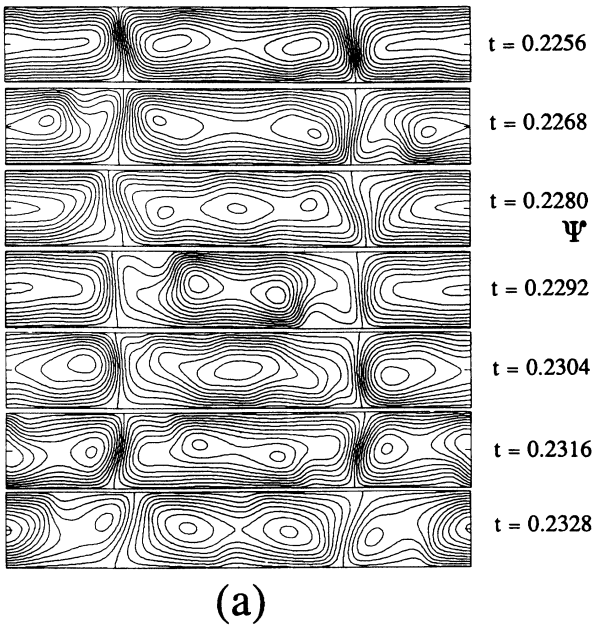


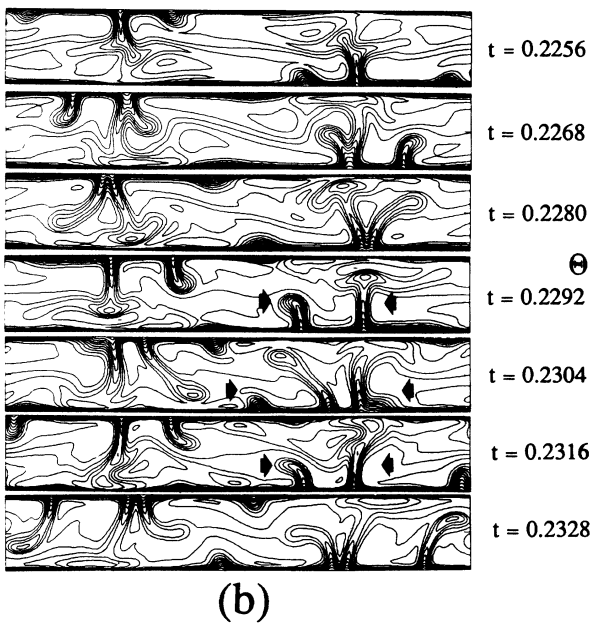


FIG. 1. Chaotic single-cell dynamics in the physical space. (a) Stream function. Time steps are given in the figure. (b) Temperature field. Evolution of the plume configuration in the boundary layer. Time has been nondimensionalized by $d^2/\kappa$, where $\kappa$ is the thermal diffusivity of the layer.

We display the two-dimensional spectrum of the nonlinear-source term $\mathbf{v}\cdot\nabla\theta$ in Fig. 3 at $t=0.204$. The presence of the bubble in the center of the spectrum shows that both the horizontal and the vertical symmetries are broken. This perturbation propagates rapidly toward large scales and eventually disappears. We note that this perturbation is not related to numerical truncation effects because it appears near the center of the spectrum and not near the borders. This bubble occurs at the instant, just before and during the disintegration of the single-cell pattern. Thus it is the spectral signal of a true physical event.

We will now introduce the concept of "thermal attractor" from the pictures shown in Fig. 1. We note that the upper and lower boundary layers have mirror symmetry about the midvertical plane. Therefore we will just focus on the event of the lower boundary layer. In the temperature fields of Fig. 1(b) we observe that the small plumes associated with the center cell move toward the right and those associated with the lateral cell move toward the left (see arrows). They appear to be pushed by the two countercirculations. But we wish to take a different point of view here and suppose that they are "attracted" toward one another. We take the thermal point of view because the thermal mechanism is at the heart of nonlinear mechanisms in infinite-Prandtl-number convection. These plumes are attracted by their common "centroid" inside the boundary layer. This "center of mass" moves only slightly, as the cells move relatively to one another [Fig. 1(a)]. It behaves like a thermal attractor in the physical space.

A direct cascade occurs, when a plume is created within the boundary layer, as the energy is transferred from the large-scale flow to the smaller features with thermal origins [see $t=0.2280$ in Fig. 1(b)]. An inverse cascade takes place when a small plume traveling along the boundary layer reaches the thermal attractor and is absorbed by it [see $t=0.2304$ in Fig. 1(b)]. A direct cascade seems to be occurring continuously, while an inverse cascade seems to occur only when the attractor attains a certain critical size.

It is important to consider the partitioning of energy for the various modes. Figure 4 shows the comparative evolution for the first five modes $E(k)$ of the vertically averaged kinetic energy, where $k$ is the dimensionless horizontal wave number. We have adopted this definition for describing the energy because issues concerning the stability of single cells are basically restricted to the horizontal direction. This definition is more appropriate than the classical averaging over a shell in the case of turbulence studies. An inverse cascade occurs when the ratio $E(k=1)/E(k=3)$ is a maximum and direct cascade takes place, when this ratio is a minimum. The single-cell chaos is characterized by a competition between the first and third harmonics (see Fig. 4). When the ratio $E(k=1)/E(k=3)$ reaches a maximum, the most important portion of the total energy is concentrat-

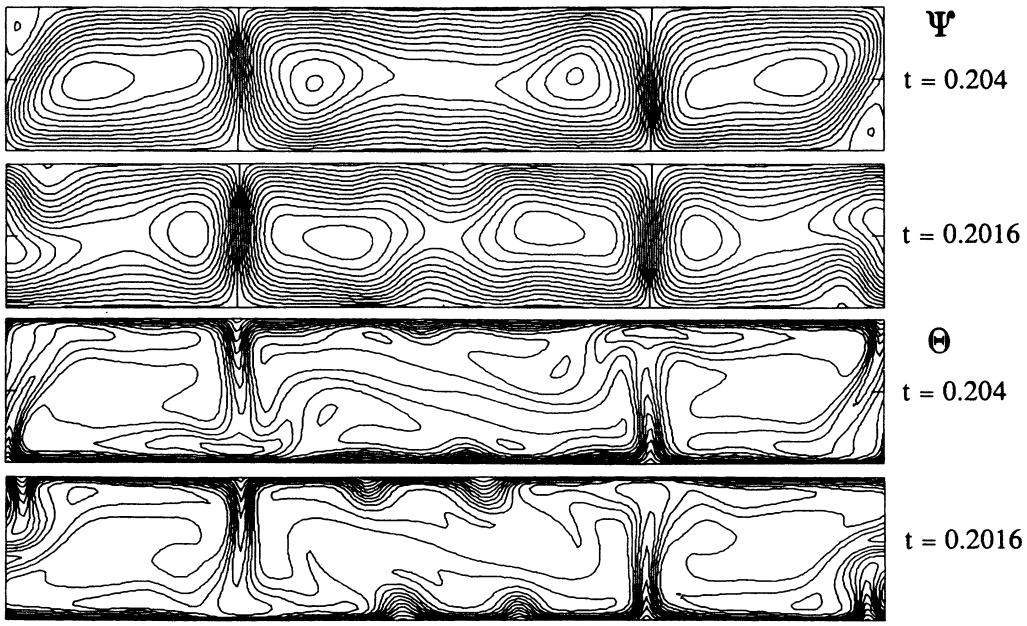


FIG. 2. Chaotic single-cell dynamics. Stream function and temperature are presented at given time intervals indicated in the figure.

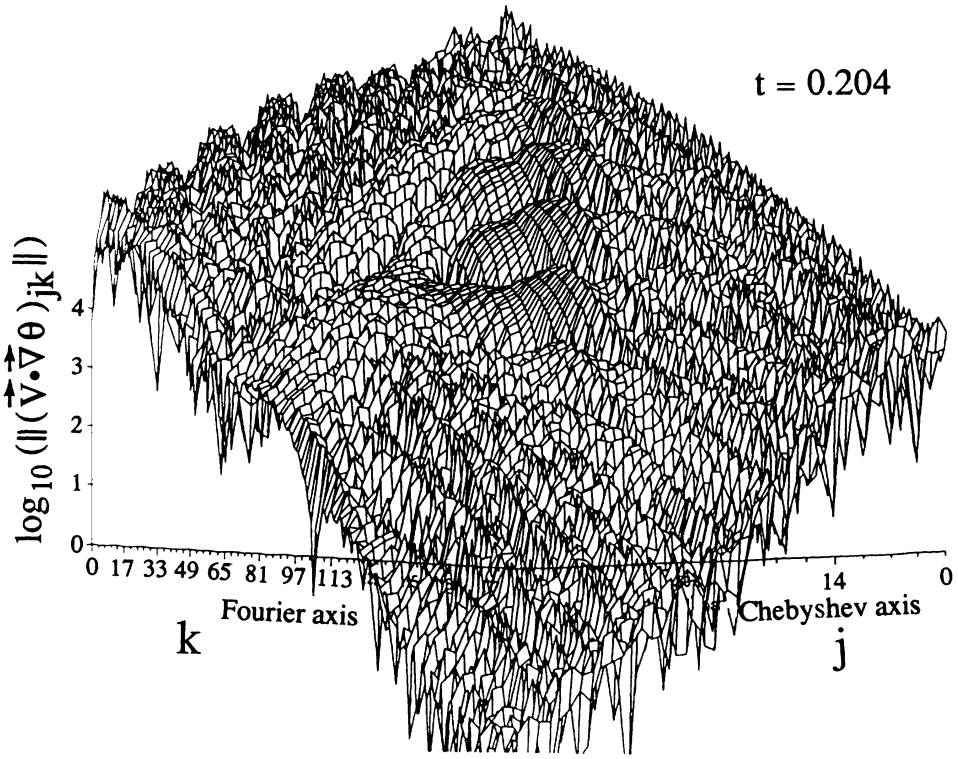


FIG. 3. Spectrum of thermal advection at $t = 0.204$. The complex norm of each Fourier-Chebyshev harmonic is displayed here. A bubble appears near the center of the spectrum.

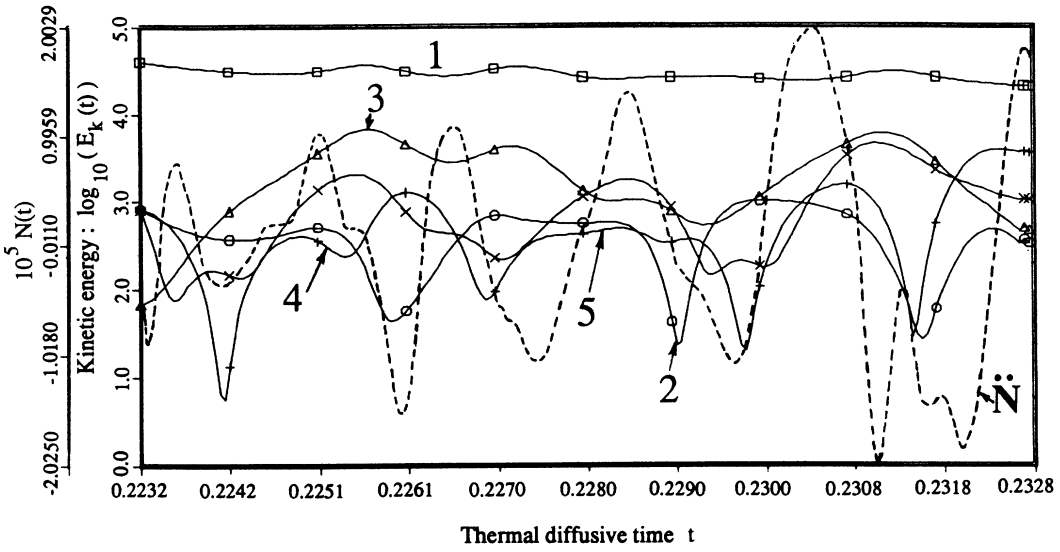


FIG. 4. Time evolution for the first five modes of the vertically averaged kinetic energy and for the second derivative of the Nusselt number.

ed in the single-cell phenomenon. This takes place when all of the plumes have nearly disappeared by collapsing into the thermal attractor [Fig. 1(b), $t=0.2268$]. In this case energy is transferred from small to large scales or an inverse cascade.

Adjacent to these curves is plotted the second derivative of the Nusselt number $N$, which is the ratio of the convective to conductive heat fluxes and is a measure of the efficiency of convection. Direct and inverse cascades are observed to occur when $d^2N/dt^2$ becomes, respectively, negative or positive. However, there are periods in time, between $t=0.2290$ and 0.2306, when the situation is less clear cut. The reason appears to be that the two cells become out of phase [Fig. 1(a)]. Thus some time is needed to reach this new equilibrium. Since the dynamics of the boundary layer can be described approximately by direct and inverse cascades, which are in turn correlated with the first two derivatives of $N(t)$, a phase-space dimension of at least 3 is needed for a proper description.

Next we consider the temporal evolution of the higher modes in Fig. 5. For $k$ greater than 10, these higher modes behave nearly the same. Modes $k=171$, 172, and 173 are shown. Each maximum is surrounded by smaller maxima. Higher-mode maxima represent direct cascades in energy, while the minima correspond to inverse cascades.

We display the evolution of the spectrum [$E(k=1)$ to $E(k=185)$] in Fig. 6(a) for $t=0.2232$ to 0.2272. The long curved structures on this energy surface correspond

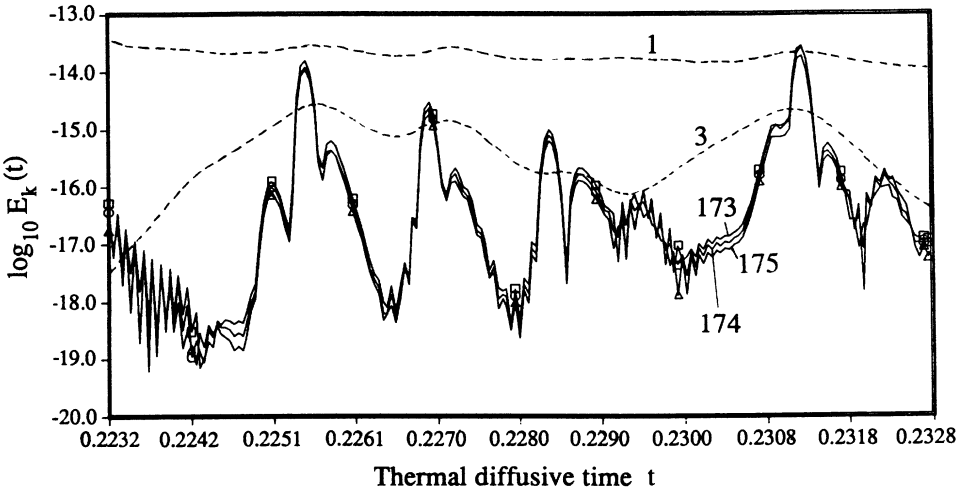


FIG. 5. Time evolution for the vertically averaged kinetic energy. Modes $k=1$, 3, 173, 174, and 175 are shown here.

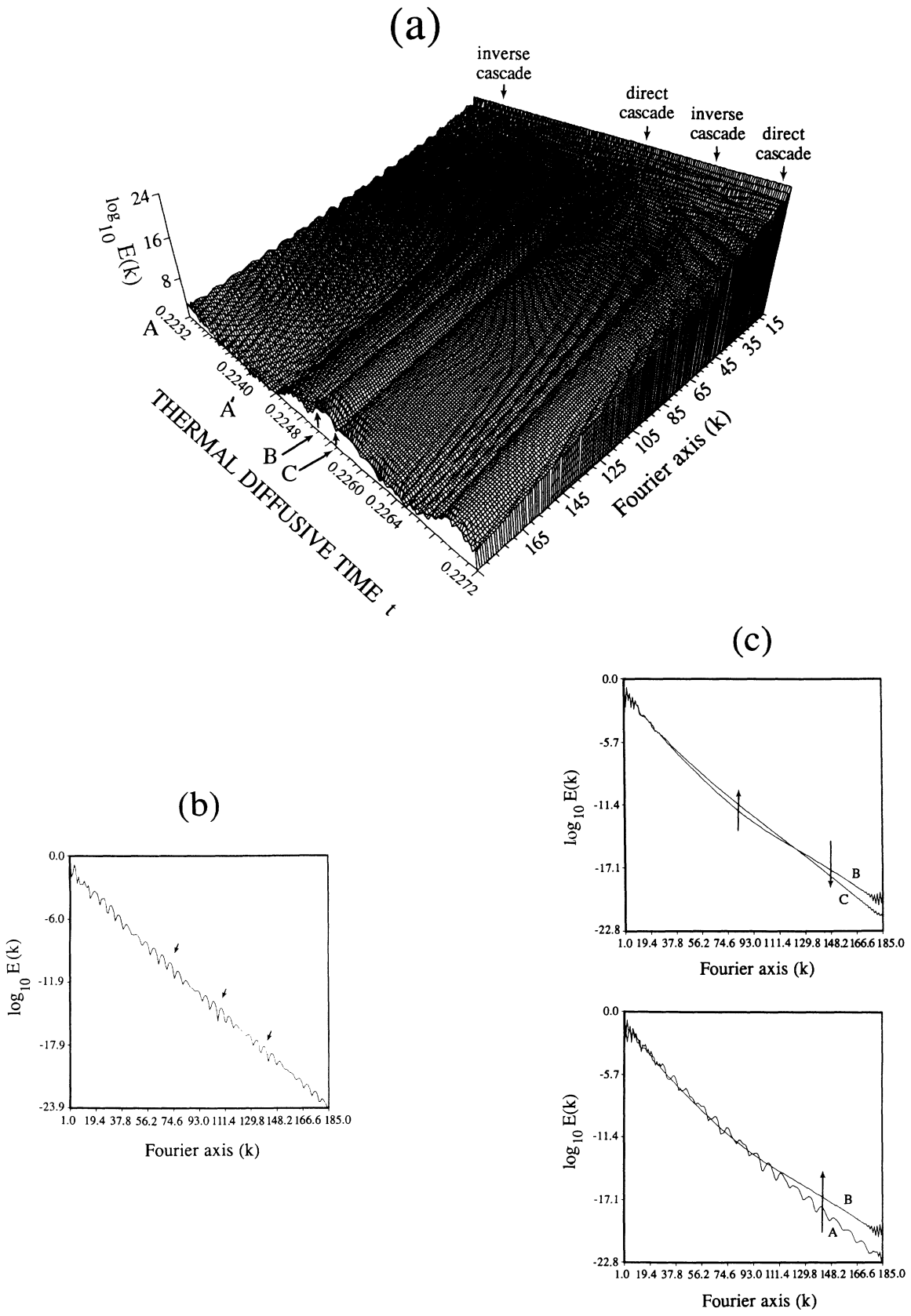


FIG. 6. Energy surface for time interval $t = 0.2232$ to 0.2272. (a) Direct and inverse cascades in energy are indicated in the figure (see arrows). (b) Cut of the energy surface at time $t = 0.2328$. Energy is transported by wave packet (see arrows) from large scales to small scales. (c) Direct cascade: Cuts of the energy surface at instants *A* and *B*. Inverse cascade: Cuts of the energy surface at instants *B* and *C*. The arrows indicate the direction of energy propagation.

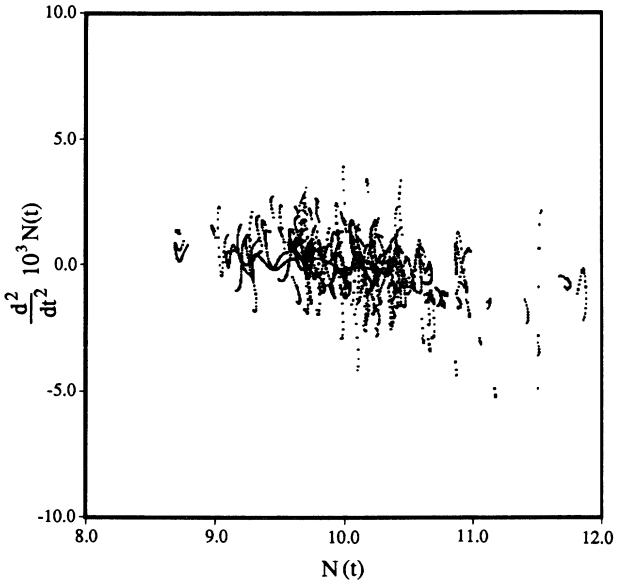


FIG. 7. Phase space. The two-dimensional $(N,\dot{N})$ topological section of the strange attractor for the period of time $t=0.1$ to $t=0.2328$ is shown here.

to direct cascades in energy, which seem to occur continuously (segment $A$-$A'$). In this way energy is transported continuously or by wave packets [Fig. 6(b)]. However, the direct cascading process seems to be interrupted randomly when these long curved structures become straight. Now the energy propagates nearly instantaneously from large to the smallest scales [Fig. 6(c)]. When this takes place, one can observe the direct cascade in the physical domain [Fig. 1(b)]. It is important to note that these long structures belong to the last part of the direct cascading process in the spectral space which is associated with the birth of a plume in the physical space.

At this time, the inverse cascade mechanism starts in the spectral domain but cannot yet be observed in the physical domain. This is shown by the cuts at instants $B$ and $C$ in Fig. 6(c). These direct and inverse cascade mechanisms begin to appear in the spectral domain sometime before they are discernible in the physical space. The underlying physical mechanism is found in the spectral domain. This example, while illustrating the spectral process, represents some inertia in the way the energy propagates. These cascades result from continuous mechanisms involving the entire spectrum. In the physical space, direct and inverse cascades can be observed when the ratio $E(k=1)/E(k=3)$ reaches, respectively, minimum and maximum values.

Since $d^2N/dt^2$ can be used to locate in time the direct and inverse cascades of energy in the physical space, we will attempt to describe these cascades in terms of a three-dimensional phase space $\{N,\dot{N},\ddot{N}\}$. Such a definition for the phase space is not the classical one commonly used in statistical physics. The definition used here is often used in nonlinear dynamics and is close to the expected fractal representation of the attractor. It is completely consistent with the computation of the fractal dimension using only one time series, e.g., $N(t)$. In short, the space $\{N,\dot{N},\ddot{N}\}$ represents the renormalized axis of the attractor. Using the algorithm of Grassberger and Proccacia[11] and 2900 points from $N(t)$, a strange attractor with fractal dimension $\nu=2.75\pm0.05$ is found. This value is characteristic of Rayleigh-Bénard convection.[12] At first one may suppose that $\nu$ probably depends upon different parameters: aspect-ratio, Prandtl number, and Rayleigh number. However, a value[12] of $\nu=2.8\pm0.1$ has also been obtained with the Proccacia-Grassberger algorithm. These determinations were based on experiments[13] done in fluids with Prandtl number 40 (silicone oil) and aspect-ratios of 1.2 and 2. For infinite-Prandtl-number fluids, Machetel and Yuen[8] found $\nu$ to be $2.8\pm0.05$ in numerical simulations of spherical-shell

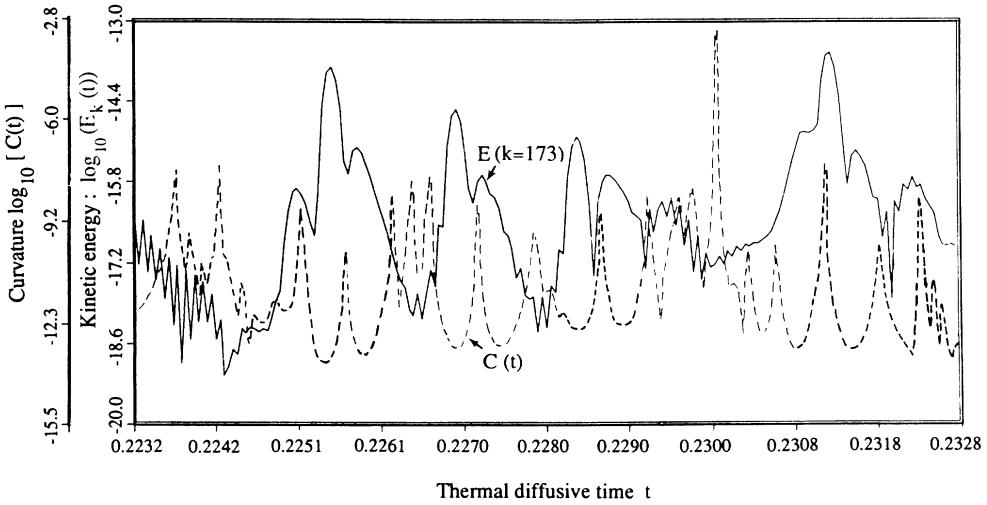


FIG. 8. Time evolution of the curvature $C(t)$ of the phase-space trajectory is shown here with the vertically averaged kinetic energy for the mode $k=173$.

thermal convection. Since the onset of the type of chaos we are dealing with is characterized by the single-cell pattern, the computed fractal dimension associated with single-cell chaos seems to lie below 3 from these three cases. Until now there has been no systematic study of the dependence of the fractal dimension on the Rayleigh number in thermal convection.

A view of this strange attractor is shown in Fig. 7. Here we have shown a section of given thickness in the center of this attractor. This vista allows the visualization of the local topological structure. A degenerate torus can be made out. This can be explained by the fact the transition to chaos in this problem is obtained via a transition from a torus with two incommensurate frequencies.[8]

In order to demonstrate a relationship between the cascading processes and the dynamics in the phase space, we plot in Fig. 8 the fine details of the time history of the highest modes (e.g., $k=173$) along side with the temporal evolution of the curvature of the attractor solution in the three-dimensional phase space. Curvature is defined here as the inverse of the radius of curvature. This quantity has been computed by using a classical formula for geometry in three-dimensional space. We observe that there is indeed a correlation between the inverse cascade, as shown by the kinetic energy, and the maxima in the curvature of the phase-space trajectory (viz., Fig. 8). This has also been found by plotting the temporal evolution of the highest modes and the time history of the associated curvature. We find that the maxima of the curvature occur when the inverse cascade starts to appear in the spectral domain. The result is the underlying focus of this work. We have thus identified the thermal attractor in the physical space to be a representative of the strange attractor in the phase space.

Up to now, chaotic convection cannot be explained fully from arguments drawn just from the physical domain. On the other hand, we can understand chaos better from considerations of a strange attractor in the phase space. In this study we have shown that relatively few derivatives of the phase-space solution are needed for a complete description of thermal chaos associated with high-Prandtl-number convection. In short, this strange attractor governs the dynamics of the thermal attractor in the physical domain. This result leads to three ordinary differential equations describing the trajectory of the solution in the three-dimensional phase space.

This research was partially supported by NASA Grant No. NAGW-1008 and by National Science Foundation Grant No. EAR-8511200.

[1]J. P. Gollub, in *Nonlinear Dynamics and Turbulence,* edited by G. I. Barenblatt *et al.* (Pitman, New York, 1983).

[2]J. P. Gollub and S. V. Benson, J. Fluid Mech. **100**, 449 (1980).

[3]F. H. Busse, in *Hydrodynamic Instabilities and the Transition to Turbulence,* 2nd ed. (Springer-Verlag, New York, 1985), pp. 97–133.

[4]G. Ahlers and R. P. Behringer, Phys. Rev. Lett. **40**, 712 (1978).

[5]R. P. Behringer, C. Agoste, J. S. Jan, and J. N. Shaumeyer, Phys. Lett. **80A**, 273 (1980).

[6]L. N. Howard and R. I. Krishnamurti, J. Fluid Mech. **170**, 385 (1986).

[7]U. R. Christensen, Geophys. Res. Lett. **14**, 220 (1987).

[8]P. Machetel and D. A. Yuen, in *Recent Developments in Seismology and Geodynamics,* edited by N. J. Vlaar *et al.* (Reidel, Dordrecht, 1988), pp. 265-290.

[9]S. Ciliberto and M. A. Rubio, Phys. Rev. Lett. **58**, 25 (1987).

[10]D. Gottlieb and S. A. Orszag, *Numerical Analysis of Spectral Methods,* CBMS-National Science Foundation Regional Conferences Series in Applied Math, No. 26 (SIAM, Philadelphia, 1977), p. 170.

[11]P. Grassberger and I. Proccacia, Phys. Rev. Lett. **50**, 346 (1983).

[12]P. Atten, J. G. Caputo, B. Malraison, and Y. Gagne, J. Mec. Theor. Appl., Special issue, p. 123 (1984).

[13]M. Dubois and P. Bergé, J. Phys. (Paris) **42**, 167 (1981).

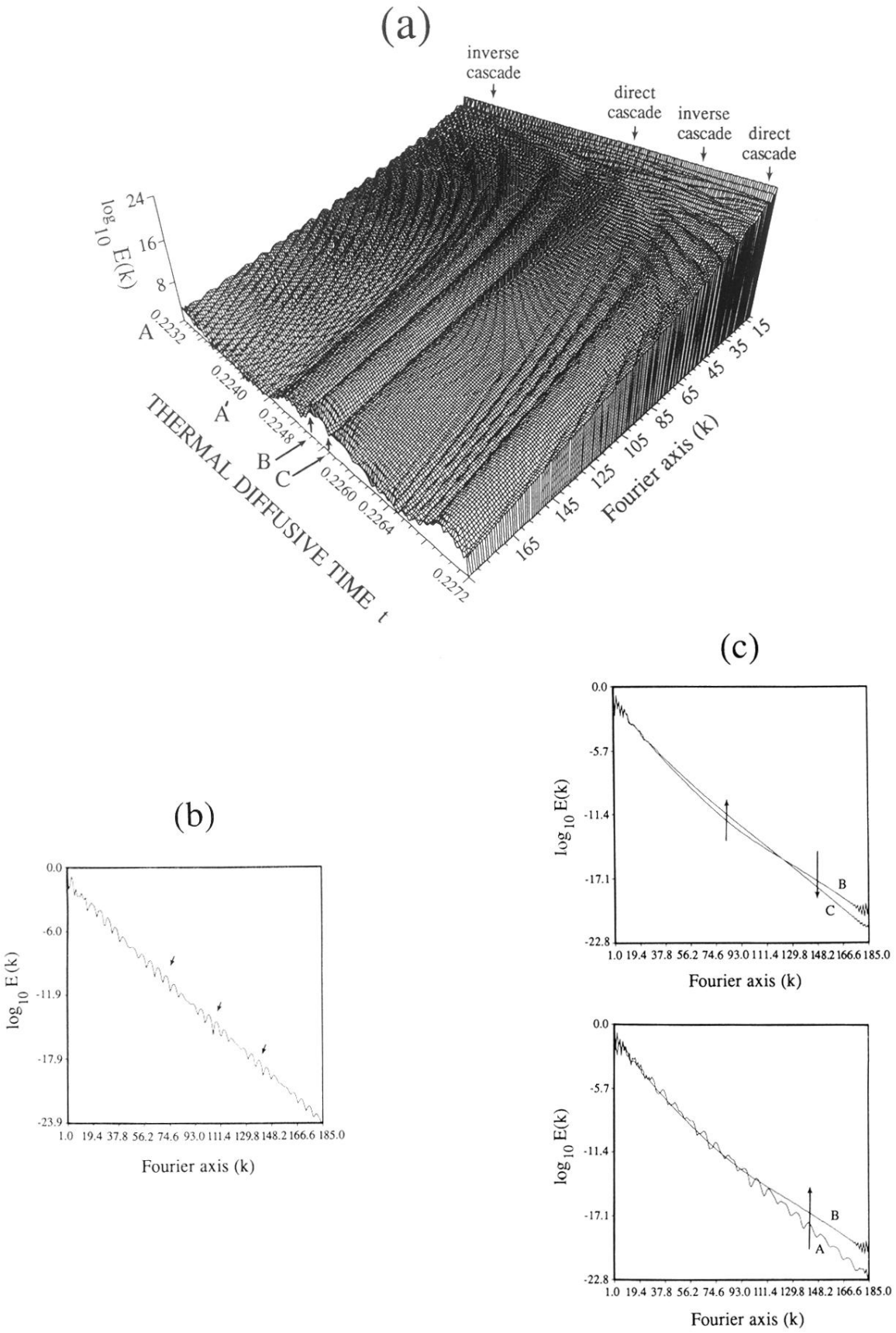


FIG. 6. Energy surface for time interval $t = 0.2232$ to 0.2272. (a) Direct and inverse cascades in energy are indicated in the figure (see arrows). (b) Cut of the energy surface at time $t = 0.2328$. Energy is transported by wave packet (see arrows) from large scales to small scales. (c) Direct cascade: Cuts of the energy surface at instants $A$ and $B$. Inverse cascade: Cuts of the energy surface at instants $B$ and $C$. The arrows indicate the direction of energy propagation.